Comparison of Pyrolysis and Combustion Properties of Rigid and Plasticized Poly(vinyl chloride)

Swann J.*, Ding Y., Stoliarov S.

University of Maryland, Department of Fire Protection Engineering, College Park, MD, USA
**Corresponding author's email: jswann91@umd.edu*

ABSTRACT

A methodology to fully parameterize a comprehensive pyrolysis model is demonstrated on specimens of plasticized and rigid poly(vinyl chloride). Thermogravimetric analysis, differential scanning calorimetry and microscale combustion calorimetry were employed to characterize the kinetics and thermodynamics of thermal decomposition and heats of complete combustion of gaseous decomposition products. Controlled Atmosphere Pyrolysis Apparatus II gasification experiments were utilized to determine the thermal transport parameters within the undecomposed material and developing char layer. A recently expanded, fully verified and validated numerical framework, ThermaKin2Ds, was employed to simulate the axisymmetric gasification experiments and analyze all experimental results. The model was shown to reproduce the experimental results with a high degree of detail. Idealistic, one-dimensional simulations of burning of solid materials in the presence of external radiant heat flux, subsequently conducted using the fully parameterized comprehensive pyrolysis models, indicated that plasticized and rigid poly(vinyl chloride) have similar mass loss rate histories. However, significant differences become apparent when the mass loss rates of gaseous decomposition products are converted to heat release rate.

KEYWORDS: Intumescence, material flammability, pyrolysis modeling, ThermaKin.

INTRODUCTION

Poly(vinyl chloride) (PVC) is a commonly used material in the built environment, which possesses desirable flammability properties. Hirschler [1] found that PVC was more difficult to ignite, easier to extinguish, more resistant to flame spread and had a lower heat release rate per unit initial mass than the majority of natural and synthetic polymers studied. The introduction of plasticizers to PVC produces flexible PVC (FPVC) to widen its range of applications, such as electrical cable [2]. The introduction of additional combustible plasticizers can alter the materials reaction to fire, which is a distinction that is often neglected in fire modeling efforts of PVC materials. Comprehensive pyrolysis modeling is important for many fire safety considerations; however, the reliability of modeling results is proportional to the accuracy of the parameters representing the materials of interest.

Our group has developed a methodology employing novel experimental tools coupled with an advanced numerical model to characterize many common materials for pyrolysis modeling [3, 4]; this methodology has recently been expanded to charring and intumescent materials [5, 6]. Thermogravimetric analysis (TGA) and differential scanning calorimetry (DSC) techniques were coupled with a comprehensive pyrolysis solver, ThermaKin, to characterize the kinetics and thermodynamics of thermal decomposition through inverse analysis. Microscale combustion calorimetry (MCC) was employed to parameterize the heats of complete combustion of pyrolyzate gases. Newly developed gasification experiments [5] were conducted to determine thermal transport parameters within the pyrolyzing samples, also analyzed through inverse analyses. This

Proceedings of the Ninth International Seminar on Fire and Explosion Hazards (ISFEH9), pp. 1109-1121
Edited by Snegirev A., Liu N.A., Tamanini F., Bradley D., Molkov V., and Chaumeix N.
Published by Saint-Petersburg Polytechnic University Press
ISBN: 978-5-7422-6498-9 DOI: 10.18720/spbpu/2/k19-50

methodology permits a comprehensive characterization of charring and intumescent materials and their associated reaction to fire. The objective of this study was to demonstrate this methodology to characterize FPVC for comprehensive pyrolysis modeling as well as provide a meaningful comparison between the fire behavior of FPVC and a rigid PVC studied previously [6].

EXPERIMENTAL AND NUMERICAL METHODS

Materials

A transparent FPVC was studied in this work. The FPVC samples were obtained from TMI Vinyl Solutions in $5.45 \cdot 10^{-3}$ m thick sheets and had a density computed at room temperature of 1226 kg/m^3. The milligram-scale test samples were carefully cut into very small flat pieces approximately 4–7 mg in mass. The samples for the gasification tests were cut to 0.07 m diameter disks using a computer numerical control (CNC) milling machine. Samples for the absorption coefficient measurements (discussed in a later section) were manufactured by machining the 0.07 m diameter disks to a thickness of $1 \cdot 10^{-3}$ m in the center (0.02 m diameter) portion of the specimen. All samples were stored in a desiccator for a minimum of 48 h prior to testing. The pyrolytic behavior of this FPVC material was compared to a pure rigid PVC studied previously [6].

Milligram-scale experiments

TGA and DSC tests were conducted simultaneously using a Netzsch 449 F3 Jupiter Simultaneous Thermal Analyzer (STA) to characterize the kinetics and thermodynamics of thermal decomposition. The temperature program for all STA tests consisted of a conditioning period, with the sample maintained at 313 K for 25 min, followed by a linear heating to 973 K. The STA tests of FPVC used in the reaction model development (see Table 1) were conducted at 10 K/min and repeated 10 times to accumulate the necessary statistics. Additional TGA tests were performed in triplicate at 5 and 20 K/min to verify that the developed reaction model correctly extrapolates the material's behavior to alternate thermal conditions. All the tests were performed in a nitrogen environment. Platinum-rhodium crucibles with lids containing a small opening were used for all STA tests to maximize temperature uniformity and heat flow sensitivity. The sample mass and heat flow data were collected as a function of time and pyrolyzing sample temperature. A detailed description of the instrument calibration and testing protocol can be found in an earlier publication [7].

MCC is a standardized test method employed to measure the heat release rate (HRR) associated with a complete combustion of gaseous products generated by a thermally decomposing solid as a function of time and solid sample temperature [8]. All MCC tests were conducted using a nominal heating rate of 10 K/min in the pyrolyzer to facilitate direct comparison with STA data. The samples were heated within the pyrolyzer in an open ceramic crucible within a fully anaerobic environment. The gaseous pyrolyzate was then mixed with excess oxygen and oxidized in the combustor. The temperature of the combustor was set at 1173 K to ensure completeness of the oxidation process. The heat released during oxidation was measured using the oxygen consumption principle [9]. The MCC apparatus was carefully calibrated on a weekly basis following recommended procedures [9]. All MCC tests on FPVC were conducted in triplicate due to a high degree of reproducibility.

Gram-scale experiments

The radiation absorption coefficient measurement was based on a methodology described by Linteris et al. [10]. A well-defined radiant heat flux from an electric conical heater was transmitted through the FPVC sample, positioned 0.07 m below the base of the heater housing, and subsequently measured with a water-cooled Schmidt-Boelter heat flux transducer. The incoming radiation was collimated by Kaowool PM insulation board to direct it through a thin ($\approx 1 \cdot 10^{-3}$ m)

portion of the specimen. All measurements were performed at a heater temperature of 940 K, which corresponded to an incident radiant heat flux of 45 kW/m^2 at a distance of 0.04 m below the heater housing. The transmitted heat flux was averaged for the first 3 s of sample exposure. Absorption coefficient tests were conducted in duplicate. The emissivity required to compute the absorption coefficient was obtained from literature. Details of the absorption coefficient measurement methodology can be found elsewhere [4, 11].

Gasification tests were conducted using the newly developed Controlled Atmosphere Pyrolysis Apparatus II (CAPA II), which enables carefully controlled pyrolysis utilizing water-cooled chamber walls. The disk-shaped samples were subjected to a nominal radiative heat flux of 30 and 60 kW/m^2. The radiative heat flux was carefully characterized to account for changes in this heat flux incident to the top sample surface due to the evolving shape and position of the sample surface associated with intumescence. All tests were conducted in duplicate in a nitrogen environment (O_2 volumetric fraction < 1%) until no mass loss was observed. The samples mass, spatially resolved bottom surface temperature and sample profile evolution were collected as a function of time. Additional information on the instrument characterization and application can be found elsewhere [5, 6].

Numerical modeling

A comprehensive pyrolysis solver, ThermaKin [12, 13], was employed to inversely analyze all experimental data and make predictions. The solver, a new version of which was named ThermaKin2Ds, was recently expanded to include a new 2Dax module capable of simulating two-dimensional axisymmetric objects [6]. ThermaKin2Ds solves for the transient rate of gaseous fuel production using fundamental physical and chemical properties of constituents of a pyrolyzing object exposed to external heat. An arbitrary reaction mechanism, consisting of first- and second-order chemical reactions, can be defined using the Arrhenius expression for the reaction rate constants.

In the modeling of the milligram-scale experiments, all samples were treated as thermally thin and simulated using a single element. The element temperature was forced to follow the experimental temperature profile by defining a sufficiently high convection coefficient, $1 \cdot 10^5$ W/(m^2·K), at the boundary. The experimental temperature profile was prescribed by expressing the heating rate via an exponentially decaying sinusoidal function to account for the variation in the instantaneous experimental heating rate with time, as explained in detail elsewhere [4, 14]. The mass flow boundary conditions were defined such that the gaseous pyrolyzate instantaneously escaped the element.

The modeling of the bench-scale (CAPA II) experiments was carried out using the 2Dax module of ThermaKin2Ds. The 2Dax module was employed by defining a single computational element in the radial direction to represent a one-dimensional (1D) simulation or by defining 10 elements in the radial direction to represent a two-dimensional (2D) simulation, which took into account non-uniform swelling of the CAPA II sample. The elements were characterized by size Δx for 1D, and Δx (axial) and Δz (radial) for 2D simulations. Each element was characterized by the component masses and temperature, which were calculated for each time step. A detailed description of this integration procedure can be found in earlier publications [12, 13].

All calculations were conducted using $\Delta x = 5 \cdot 10^{-5}$ m and $\Delta z = 3.5 \cdot 10^{-3}$ m (2D model only) spatial discretization and 0.01 s time step. Increasing or decreasing these integration parameters by a factor of 2 did not produce any significant changes in the results of the simulations, indicating convergence of the numerical solutions. The gaseous products were assumed not to contribute to the volume of the sample in all simulations conducted in this work. The prescribed density of each decomposition product was decreased systematically to model the expansion of the intumescent

sample. The external thermal boundary conditions were implemented to emulate those in the CAPA II experimental setup. Additional information on the modeling methodology can be found elsewhere [6].

RESULTS AND DISCUSSION

Overall methodology

The following methodology, consisting of three consecutive steps, was employed to characterize FPVC pyrolysis. The first step included milligram-scale experiments, which decoupled thermal decomposition from thermal transport to enable the determination of the kinetics and thermodynamics of thermal decomposition and the heats of complete combustion of gaseous decomposition products through manually iterative inverse analyses. The second step employed gram-scale gasification experimental results to characterize the density and thermal conductivity of each condensed-phase component through a manually iterative inverse analysis procedure. Throughout the parameterization process, an attempt was made to minimize the number of independent parameters and thus create the simplest model that captures the experimental data with the accuracy comparable to their uncertainty. The third step utilized CAPA II MLR histories obtained at a range of external heating intensities to validate the parameterized pyrolysis model. This methodology is a hierarchical process which relies on the results of previous steps to enable a well-posed mathematical problem ensuring a single solution at each step. The resulting FPVC pyrolysis model and the rigid PVC model from an earlier work [6] were compared to determine the impact of plasticizers on the material's reaction to fire.

Inverse analysis of milligram-scale experiments

The mean experimental TGA and DSC data are presented as symbols in Fig. 1. The instantaneous mass, m, and associated mass loss rate, MLR, normalized by the initial mass, m_0, as a function of temperature, T, are shown in Fig. 1(a). The heat flow to the sample and integral heat flow, both normalized by the initial mass, are presented as a function of temperature in Fig. 1(b). Here, all positive values of heat flow represent endothermic processes. The error was calculated from the scatter of the data as two standard deviations of the mean (some error bars are difficult to discern because they are comparable in size to the data symbols). The experimental MLR profile contains two prominent peaks, the first at 586 K and the second at 740 K, corresponding to the thermal decomposition process. The decomposition produced 6.4 wt.% of final condensed-phase residue. The heat flow curve contains two distinct maxima that closely correspond to the MLR profile.

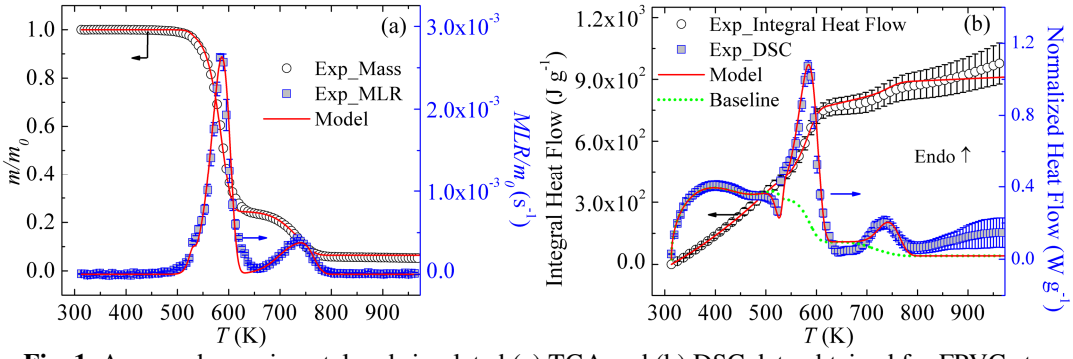

Fig. 1. Averaged experimental and simulated (a) TGA and (b) DSC data obtained for FPVC at a nominal heating rate of 10 K/min.

Inverse modeling of the STA data was performed using the approach described in detail in earlier

publications [7, 14-17]. The stoichiometric coefficients and Arrhenius parameters of a single first-order reaction was initially employed to model the TGA data. The parameters were refined through a manually iterative process using ThermaKin2Ds until the modeling results were found to be in agreement with the experimental data. The agreement was declared satisfactory when the differences between the average experimental and modeled final mass residues, and temperatures and magnitudes of MLR maxima were found to be within 3%, 5 K and 8%, respectively. If it was impossible to achieve such agreement, an additional reaction was added to the reaction scheme and its parameters were adjusted iteratively to achieve further improvement. In the case of FPVC, four consecutive reactions, Reactions 1 to 4, were required to capture the intricacies of the initial rise, multiple maxima and final decay of the MLR within the accuracy of the experimental data. This series of first-order reactions are provided in Table 1 and the resulting model is shown in Fig. 1 as solid lines. The resulting reaction scheme was validated by predicting the temperatures and magnitudes of the MLR maxima within 10 K and 13%, respectively, of the average TGA experimental data collected at 5 and 20 K/min.

Table 1. Reaction scheme and kinetic parameters for the thermal decomposition of FPVC. A negative value for heats of decomposition (h) represents endothermic processes

#	Reaction	A, s^{-1}	E, J/mol	H, J/kg
1	FPVC → 0.98 FPVC_Res1 + 0.02 FPVC_Gas1	$1.5 \cdot 10^{32}$	$3.41 \cdot 10^{5}$	$1.8 \cdot 10^{4}$
2	FPVC_Res1 → 0.25 FPVC_Res2 + 0.75 FPVC_Gas2	$7.0 \cdot 10^{11}$	$1.56 \cdot 10^{5}$	$-2.5 \cdot 10^{5}$
3	FPVC_Res2 → 0.75 FPVC_Res3 + 0.25 FPVC_Gas3	$3.0 \cdot 10^{10}$	$1.70 \cdot 10^{5}$	$-1.0 \cdot 10^{4}$
4	FPVC_Res3 → 0.35 FPVC_ Res4 + 0.65 FPVC_Gas4	$3.0 \cdot 10^{10}$	$1.80 \cdot 10^{5}$	$-3.0 \cdot 10^{5}$

The heat flow data were analyzed by first focusing on the regions not associated with melting or decomposition. The data corresponding to these regions were divided by the instantaneous heating rate and fitted with linear functions representing heat capacities, c, of the corresponding condensed-phase components. The heat flow data between 313 and 500 K were used to determine the heat capacity of undecomposed FPVC. Due to the small residual char yield, the heat capacity of FPVC_Res4 was prescribed to be the average heat capacity of chars generated by several representative charring polymers [15]. It was assumed that the heat capacity of FPVC_Res3 was identical to FPVC_Res4 due to the reaction occurring at a similar temperature range. The heat capacity of the remaining intermediate condensed-phase products (FPVC_Res1 and FPVC_Res2) were assumed identical and equal to the average heat capacity of FPVC and FPVC_ Res4 to reduce the number of independently adjustable parameters. All heat capacity values are listed in Table 2. The heat capacity of all gaseous decomposition products were assumed equal to 2100 J/(kg·K), which was the mean heat capacity of a collection of C1 to C8 hydrocarbons at a temperature of 600 K [18]. The value of this heat capacity had negligible impact on the presented modeling results.

Table 2. Heat capacities of condensed-phase components for FPVC decomposition

Component	c, J/(kg·K)	Component	c, J/(kg·K)
FPVC	$-221 + 5.10T$	FPVC_Res3	1700
FPVC_Res1	$739.5 + 2.55T$	FPVC_Res4	1700
FPVC_Res2	$739.5 + 2.55T$		

The sensible heat flow baseline was subsequently calculated as a product of the mass fractions of condensed-phase components (whose temporal evolution was computed by ThermaKin2Ds), corresponding heat capacities and instantaneous heating rate. The baseline obtained for FPVC is shown as a dotted line in Fig. 1(b). Subtraction of this baseline from the normalized experimental heat flow and subsequent integration of the differences yielded the values of the heats of decomposition, h. The heats of decomposition were subsequently refined until the simulated heat flow maxima were within 10%, temperatures of the maxima were within 8 K and the final integral heat flow value was within 5% of the corresponding experimental data. The results of this exercise are shown as solid lines in Fig. 1(b). The heats of decomposition are listed in Table 1.

The mean experimental MCC HRR and total heat release (THR) data, both normalized by the initial FPVC sample mass, are presented as a function of temperature in Fig. 2. The heats of combustion, h_c, of gaseous components defined in the reaction mechanism (see Table 1) were determined through simulating the HRR curves. Initial comparisons between the experimental HRR and modeled MLR profiles generated using the heating rate history specific to the MCC revealed some discrepancies. These discrepancies were identified through a recognition that any significant heat release should require a concurrent mass loss. These discrepancies were attributed to sample temperature deviations from that measured by the MCC sensor and were corrected by shifting the experimental curves to a slightly higher temperature, as shown in Fig. 2.

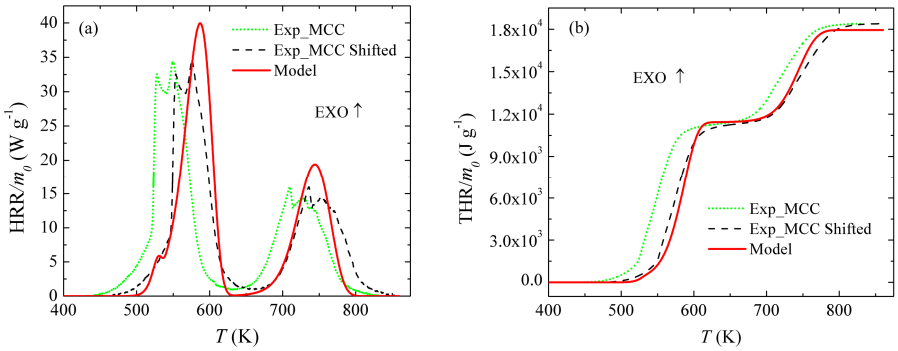

Fig. 2. Mean experimental and simulated normalized (a) heat release rate and (b) total heat release from MCC tests on FPVC at a nominal heating rate of 10 K/min.

The heats of combustion were first estimated by dividing the shifted experimental HRR data by the rate of production of gaseous components computed by ThermaKin2Ds. A simulated HRR curve was subsequently generated using the estimated h_c values. The values of h_c were further refined until the simulated and experimental HRR and THR data agreed within established MCC criteria. The criteria were defined as differences of less than 8% between the height of the experimental and modeled HRR maxima, less than 10 K between the temperatures of the maxima, and less than 8% between the final integral HRR values. The resulting heats of combustion are shown in Table 3. The simulated MCC data, using these h_c values, is shown as solid lines in Fig. 2.

Table 3. Heats of complete combustion of FPVC gaseous decomposition products (positive values represent exothermic processes)

Component	h_c, J/kg	Component	h_c, J/kg
FPVC_Gas1	$2.70 \cdot 10^7$	FPVC_Gas3	$1.20 \cdot 10^7$
FPVC_Gas2	$1.39 \cdot 10^7$	FPVC_Gas4	$4.90 \cdot 10^7$

Analysis of gram-scale experiments

Analysis of the gram-scale tests requires knowledge of the emissivity and absorption coefficients *a priori*. The initial emissivity of FPVC (0.90) was assumed to be equal to rigid PVC and was obtained from literature [19]. The emissivity of FPVC_Res4 (0.94), and thus FPVC_Res3, was estimated based on independent tests described elsewhere [6]. The remaining reactants, FPVC_Res1 and FPVC_Res2, were prescribed to have the average emissivity of FPVC and FPVC_Res4. The absorption coefficient of virgin FPVC, normalized by its density at ambient temperature, was estimated to be 1.1 ± 0.2 m^2/kg based on measurements performed in the current study. The upper char layer was observed to appear very optically dark and graphitic in nature. Therefore, the absorption coefficient of FPVC_Res4 was defined sufficiently high (100 m^2/kg) such that all the radiation was absorbed at the top surface. The absorption coefficient of FPVC_Res1 and FPVC_Res2 were defined to be the average of FPVC and FPVC_Res4.

The experimental CAPA II dataset for FPVC pyrolysis, at a nominal heat flux of 30 and 60 kW/m^2, are shown in Fig. 3 and Fig. 4. Representative shape profiles are provided in Fig. 3 as a function of time, t. The bottom surface temperature histories of the center (r_z/R = 0) and edge (r_z/R = 0.86) of the sample are presented as symbols in Fig. 4(a)(c), where r_z is the instantaneous sample radius and R is the initial total sample radius. The mean experimental MLR is shown in Fig. 4(b)(d). The uncertainty was computed from the scatter of the data as two standard deviations of the mean. The modeling results, also presented in Fig.3 and Fig. 4, are discussed in a later portion of the manuscript.

The sample's swelling process includes simultaneous increase in thickness and reduction in diameter at later stages of decomposition. At all heat fluxes, the increase in thickness is monotonic. The bottom surface temperature is spatially uniform in the early stages of pyrolysis. In later stages, the temperature becomes non-uniform with the edge of the surface being systematically cooler than the center. The MLR data at 30 kW/m^2 exhibit a single prominent peak, while the 60 kW/m^2 MLR data exhibit multiple peaks during pyrolysis.

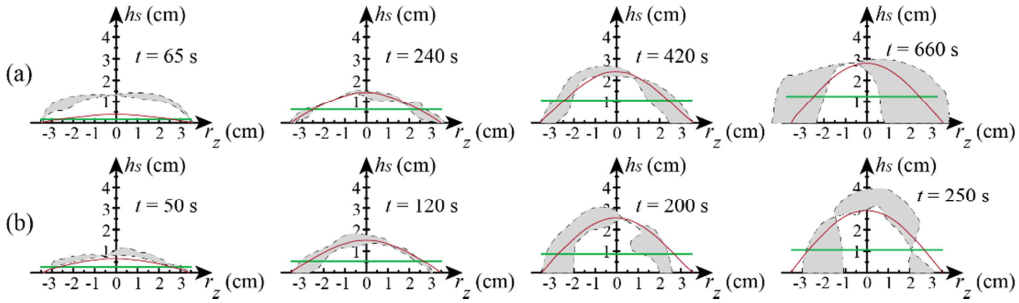

Fig. 3. The black dashed lines are experimental data from duplicate FPVC tests at (a) 30 kW/m^2 and (b) 60 kW/m^2. The vertical axis (h_S) begins at the initial position of the top sample surface. The shaded area indicates the profiles uncertainty. The straight and curved solid lines represent 1D and 2D model results, respectively.

In the following gram-scale model characterization, the 30 kW/m^2 shape profile and temperature dataset is employed as fitting targets; therefore, the 60 kW/m^2 dataset is strictly used as validation for the resulting model. The intumescent behavior of the FPVC pyrolysis was captured numerically in ThermaKin2Ds by prescribing decreasing component densities to account for increased sample thicknesses. In the 1D simulation, the sample thickness expanded uniformly across the entire radius; therefore, the average experimental sample thickness was employed as a target value for the density parametrization. The densities were decreased through a manually iterative procedure such that the

fitted sample thickness (solid straight line) captured the critical shape changes in the 30 kW/m^2 dataset, shown in Fig. 3(a). The densities also factored in reductions in mass associated with the individual reaction steps (listed in Table 1). The densities of each reactant of 1D FPVC pyrolysis are provided in Table 4. The density parameterization was dependent upon the thermal transport parameters; therefore, the density and thermal conductivity parameters were iteratively adjusted simultaneously until satisfactory results were obtained

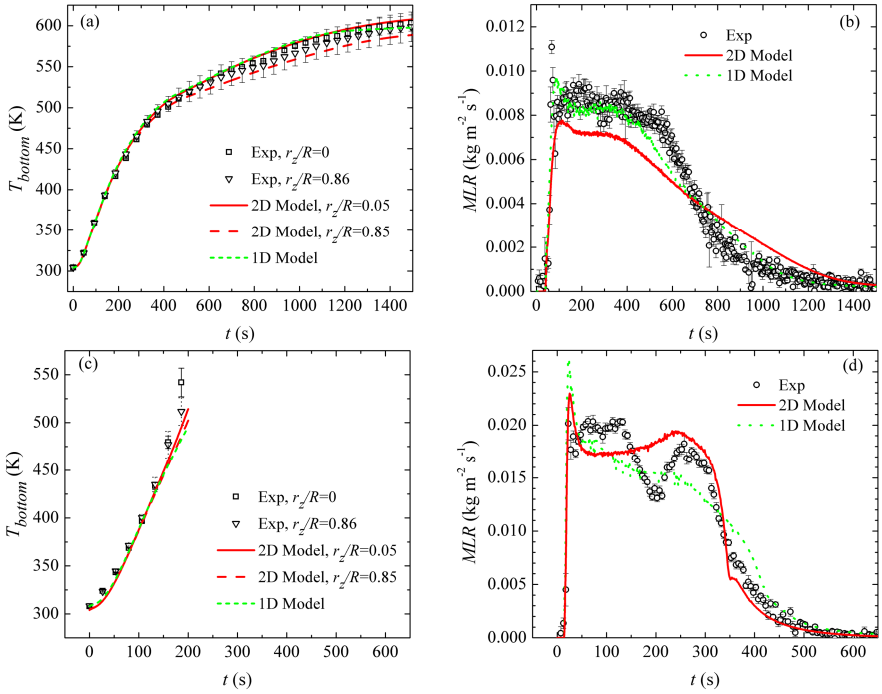

Fig. 4. Averaged experimental and modeled bottom surface temperatures and MLR data obtained at (a)(b) 30 kW/m^2 and (c)(d) 60 kW/m^2. The 60 kW/m^2 temperature data was truncated during later stages of pyrolysis due to the sample decoupling from the copper foil, resulting in poor thermal contact and unreliable data.

The average bottom surface temperature of the 30 kW/m^2 dataset was employed as target data for the inverse analysis of the thermal transport parameterization of the 1D model. The thermal conductivity of each component was first defined as a constant value, to maintain the simplest model possible. However, it was identified that a constant thermal conductivity was unable to capture the temperature history of the sample. Therefore, additional complexity was added through the introduction of a constant term multiplied by the third power of temperature; this term was only introduced to FPVC_Res3 and FPVC_Res4. The third power of temperature is an approximation to capture the thermal transport within porous media through radiation diffusion [20]; therefore, it was only physically meaningful to apply to components that experience a high temperature and porous structure. The resulting fitted bottom surface temperature is shown as the dotted line in Fig. 4(a). The final thermal conductivities are provided in Table 4. The predicted bottom surface temperature for the 60 kW/m^2 dataset is shown in Fig. 4(c). The average error between the experimental and simulated bottom surface temperatures for 30 and 60 kW/m^2 was found to be 1.1 and 2.8%, respectively.

The 30 kW/m^2 MLR data, shown in Fig. 4(b), were not utilized in the inverse analysis model calibration; therefore, this dataset serves as a model validation. The 1D model predicted the

30 kW/m^2 MLR data with excellent agreement. The overall error between the experimental and modeled MLR was found to be 8.7%. The MLR prediction for the higher flux, shown in Fig. 4(d), notably underestimated the experimental MLR data. The overall error between the experimental and modeled MLR for the 60 kW/m^2 dataset was found to be 11.9%. The 1D FPVC pyrolysis model was capable of simulating the MLR with reasonable accuracy for both the 30 and 60 kW/m^2 datasets.

Table 4. Densities and thermal conductivities of condensed phase components for 1D pyrolysis model

Component	ρ, kg/m^3	k, W/(m·K)
FPVC	1226	0.12
FPVC_Res1	391	0.41
FPVC_Res2	98	0.41
FPVC_Res3	62	$0.70 + (5.0 \cdot 10^{-10}) T^3$
FPVC_Res4	22	$0.70 + (5.0 \cdot 10^{-10}) T^3$

2D modeling was subsequently performed to account for variation in the heating conditions along the sample radius and top surface non-uniformity (see Fig. 3). Similar to the 1D model parameterization, the 30 kW/m^2 experiments were employed as the target data because these experiments produced the maximum reliable data with minimal radial sample reduction during pyrolysis. In the 2D model, the radial dependence of the intumescent behavior of FPVC pyrolysis was captured more accurately by effectively defining the densities as a function of radius. To simplify the parametrization, the radial dependence was prescribed as a combination of the center and edge densities. Independent knowledge of the center and edge char expansion dynamics enabled individual parameterization of the respective densities. Two separate initial FPVC components, FPVC$_c$ (center) and FPVC$_e$ (edge), were created with identical properties. FPVC$_c$ and FPVC$_e$ were defined to follow an identical decomposition reaction scheme; however, the densities and thermal conductivities of their products of decomposition were different. Distinguishing between the center and edge enabled parameterization of the radially dependent sample shape profiles.

To capture the intumescence at the center axis, the densities were prescribed following an identical process to the 1D model development; however, the center char thicknesses were employed as fitting targets instead of the average. While fitting the center densities, the sample diameter in the model was reduced from 0.035 m to 0.02 m to ensure that the heat flux to the sample was representative of the heat flux incident to the center portion of the sample. The densities were manually adjusted until the center experimental thicknesses, shown in Fig. 3(a), were well represented. The densities for the edge components were defined such that the thickness of the sample remained constant to emulate negligible swelling, as experimentally observed, which was achieved by multiplying the density by the corresponding stoichiometric mass coefficient of each reaction. The resulting densities of all reactants are provided in Table 5 denoted by the respective subscript.

To couple the densities between the center and edge components, a profile describing the mass fraction of the center component ($mf_{\mathrm{FPVC,c}}$) was computed; details on this methodology can be found elsewhere [6]. The center component mass fraction is given as a function of sample radius, r_z (m), in Eq. (1). The summation of the center and edge mass fractions must equal unity. The radially dependent mass fraction of the center components was computed to emulate the FPVC sample shape profile at 240 s of the 30 kW/m^2 dataset, a representative shape profile. It was observed that the center of the sample was comprised entirely of the center component. As the radius increased,

the center mass fraction decreased, which resulted in the edge mass fraction increasing. The resulting sample shape profiles computed with the 2D axisymmetric model are shown in Fig. 3 as the solid curved lines. With the exception of under-estimating the initial rapid expansion in the 30 kW/m^2 dataset, it was observed that the model captured the overall dynamics of swelling with excellent accuracy.

$$mf_{\mathrm{FPVC,e}} = 1.24 \cdot 10^5 r_z^{\,4} - 9.52 \cdot 10^2 r_z^{\,2} + 1 \tag{1}$$

The thermal conductivities of the center components were parameterized following the same methodology discussed for the 1D model; however, the values were modified to capture the center experimental temperature profile instead of the average. The thermal conductivities of the edge components were scaled based on the density ratio between the center (FPVC$_c$) and edge (FPVC$_e$) components. The thermal conductivity was assumed inversely proportional to the density; therefore, the solid that expanded more upon decomposition was assumed to have proportionally larger thermal conductivity. This scaling was based on a physical argument provided in an earlier publication [21]. Consequently, the edge thermal conductivities were not fitting parameters; instead, they were directly coupled to the center parameters. The resulting temperature predictions at the center and edge of the sample are shown as the solid and dashed lines in Fig. 4(a)(c). An average error between the experimental and simulated results of the 30 and 60 kW/m^2 data was found to be 0.4 and 2.8%, respectively. The thermal conductivities of all center and edge components are shown in Table 5.

Table 5. Densities and thermal conductivities of the center (denoted by subscript c) and edge (denoted by subscript e) condensed phase components of 2D FPVC pyrolysis

Component	ρ, kg/m^3	k, W/(m·K)	Component	ρ, kg/m^3	k, W/(m·K)
FPVC$_c$	1226	0.12	FPVC$_e$	1226	0.12
FPVC$_c$_Res1	219	0.62	FPVC$_e$_Res1	1202	0.11
FPVC$_c$_Res2	55	0.62	FPVC$_e$_Res2	300	0.11
FPVC$_c$_Res3	35	$1.1 + (8.0 \cdot 10^{-9})\, T^3$	FPVC$_e$_Res3	225	$0.17 + (1.2 \cdot 10^{-9})\, T^3$
FPVC$_c$_Res4	12	$1.1 + (8.0 \cdot 10^{-9})\, T^3$	FPVC$_e$_Res4	79	$0.17 + (1.2 \cdot 10^{-9})\, T^3$

The MLR data, shown in Fig. 4(b)(d), were not utilized in the model development. The predicted MLR for the 30 kW/m^2 data was under estimated during the first 700 s and was subsequently over predicted during later stages of pyrolysis. The simulated MLR for the 60 kW/m^2 tests was found to capture the data well. The overall agreement between the experimental and 2D modeled MLR for the 30 and 60 kW/m^2 datasets were found to have a mean error of 18.7 and 14.1%, respectively.

Additionally, Fig. 4 provides a comparison between the 1D and 2D model predictions. The dotted lines represent the 1D model and the solid and dashed lines represent the 2D model. The bottom temperatures, shown in Fig. 4(a)(c), demonstrate minimal discrepancies between the two models. The MLR, however, reveals differences that are more noticeable. These differences are likely attributed to the 1D and 2D model's ability to capture the evolution of the top sample surface and its associated interactions with the radiation field. The 2D model better captures these surface interactions resulting in excellent predictions for the 60 kW/m^2 dataset. However, the 2D model under predicts the MLR at 30 kW/m^2 due to its inability to capture the rapid sample swelling during initial stages of pyrolysis.

COMPARISON BETWEEN LARGE-SCALE PLASTICIZED AND RIGID PVC MODELS

A simulation of a large burning surface exposed to radiant heat flux, emulating a large-scale fire, was conducted to compare the FPVC characterized in this work and rigid PVC studied elsewhere [6]. The simulation enabled a quantitative comparison between the predicted area-normalized large-scale mass loss rate (MLR_{LS}) and heat release rate (HRR_{LS}) of FPVC and PVC exposed to identical conditions. A $6.15 \cdot 10^{-3}$ m thick sample was subjected to a constant radiant heat flux of 40 and 70 kW/m^2 to provide a direct comparison. The convective losses from the top sample surface were neglected and the bottom sample surface employed adiabatic boundary conditions. The simulations neglected the potential impact of sample surface oxidation prior to ignition, because the condensed-phase model was parameterized based on anaerobic measurements. Moreover, the additional heat flux provided by a flame that forms on the sample surface upon ignition was also ignored in these simulations. The calculations were terminated when no additional mass loss was observed.

The large surface burning model employed the thermal transport parameters of the center components of the 2D model (see Table 5) to factor out the edge effects observed in the CAPA II [6]. The simulated HRR_{LS} was constructed as the product of the simulated MLR_{LS} of individual gaseous decomposition products from the reaction scheme (see Table 1) and the corresponding heats of combustion of each independent decomposition product derived from MCC measurements (see Table 3). It is especially critical to characterize independent heats of combustion for the decomposition products of materials like rigid PVC, where the heats of combustion of individual products differ substantially [6].

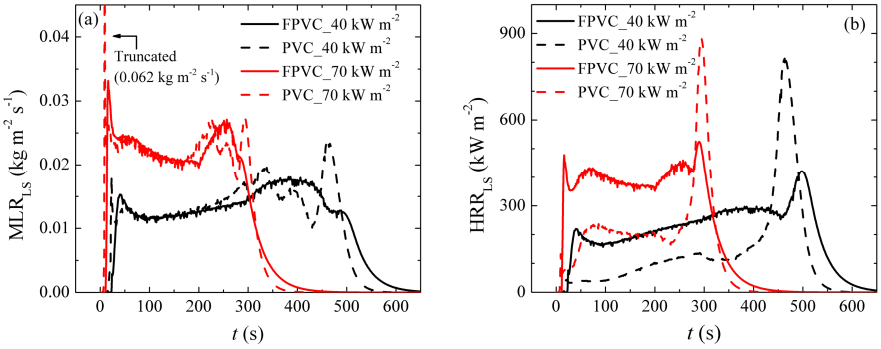

Fig. 5. Simulated (a) MLR_{LS} and (b) HRR_{LS} of FPVC and PVC, employing the center parameters from the 2D model parameterization, under a nominal heat flux of 40 and 70 kW/m^2.

A comparison between the simulated MLR_{LS} and subsequently computed HRR_{LS} of both FPVC and PVC large-scale burning is portrayed in Fig. 5. It is shown that there are negligible differences in the MLR_{LS} profiles between the two materials under both 40 and 70 kW/m^2. The HRR_{LS}, however, displays substantial differences between FPVC and PVC at both incident heat fluxes. In the early stages of burning, the HRR_{LS} of PVC is lower than that of the FPVC by a factor of two. However, during the final stages of burning, the HRR_{LS} estimated for PVC has a maximum peak that is a factor of two greater in magnitude than FPVC. Although PVC produces a greater HRR_{LS} during the final stages of burning in idealistic conditions, this peak is unlikely to contribute significantly to fire growth because it does not occur until very late stages of pyrolysis (requiring high heat flux exposure) and the extensive deformation of the burning material is expected to mitigate its reaction to fire. Therefore, the larger HRR_{LS} of FPVC during the early stages of burning will likely result in a greater flame spread rate during an actual fire event, consequently, making FPVC a greater fire hazard. Unlike rigid PVC which produces a small HRR in the first step of decomposition [6], FPVC produces a large amount of heat (see Fig. 2) which is believed to be originated from the organic

plasticizers that are added to these materials. As a result, it is imperative that these differences between FPVC and PVC are included in all modeling efforts to capture the material's unique reaction to fire.

CONCLUSIONS

This manuscript presents a systematic methodology to fully parameterize a comprehensive pyrolysis model of FPVC. The complete set of parameters was derived from a combination of milligram-scale (TGA, DSC and MCC) tests and gram-scale (CAPA II) gasification experiments, which were coupled with inverse numerical modeling using ThermaKin2Ds, a newly expanded axial symmetric modeling framework. TGA and DSC experimental data were employed to parameterize a numerical reaction model, comprised of sequential first-order reactions, capable of predicting the kinetics and thermodynamics of thermal decomposition within the accuracy of the instrumentation. The heats of complete combustion of volatile gases produced in each reaction were determined by inversely analyzing the MCC datasets. A comprehensive pyrolysis model was derived by coupling the previously determined reaction parameters with the thermal transport properties estimated from CAPA II data. The model was subsequently validated against several experimental datasets collected from outside the model calibration thermal exposure. Finally, a comparison between the developed FPVC pyrolysis model and a rigid PVC pyrolysis model developed elsewhere [6] yielded similar burning rates but substantially different heat release rates between the materials. The combustion of gaseous products originated from the organic plasticizers during the first step of FPVC decomposition is largely responsible for the significant increase in the heat release rate exhibited by FPVC, with respect to rigid PVC, early in the burning process. It should be noted that the results presented in this manuscript cannot necessarily be generalized to all commercially available flexible PVC materials as their compositions may differ significantly.

ACKNOWLEDGEMENTS

The authors would like to acknowledge this research was supported by the U.S. National Science Foundation CAREER Award #1347196 under the grant monitor Dr. Song-Charng Kong.

REFERENCES

[1] M.M. Hirschler, Poly(vinyl chloride) and its Fire Properties, Fire Mater. 41 (2017) 993–1006.

[2] T. Gong, Q. Xie, X. Huang, Fire Behaviors of Flame-Retardant Cables Part I: Decomposition, Swelling and Spontaneous Ignition, Fire Saf. J. 95 (2018) 113–121.

[3] S.I. Stoliarov, J. Li, Parameterization and Validation of Pyrolysis Models for Polymeric Materials, Fire Technol. 52 (2016) 79–91.

[4] M.B. McKinnon, S.I. Stoliarov, Pyrolysis Model Development for a Multilayer Floor Covering, Materials. 8 (2015) 6117–6153.

[5] J.D. Swann, Y. Ding, M.B. McKinnon, S.I. Stoliarov, Controlled Atmosphere Pyrolysis Apparatus II (CAPA II): A New Tool for Analysis of Pyrolysis of Charring and Intumescent Polymers, Fire Saf. J. 91 (2017) 130–139.

[6] J.D. Swann, Y. Ding, S.I. Stoliarov, Characterization of Pyrolysis and Combustion of Rigid Poly(vinyl chloride) using Two-Dimensional Modeling, Int. J. Heat Mass Transf. 132 (2019) 347-361.

[7] J. Li, S.I. Stoliarov, Measurement of Kinetics and Thermodynamics of the Thermal Degradation for Non-Charring Polymers, Combust. Flame 160 (2013) 1287–1297.

[8] ASTM International, D7309-11 Standard Test Method for Determining Flammability Characteristics of Plastics and Other Solid Materials Using Microscale Combustion Calorimetry, West Conshohocken, 2011. doi:10.1520/D7309-11.

[9] R.E. Lyon, R.N. Walters, S.I. Stoliarov, N. Safronava, Principles and Practice of Microscale Combustion Calorimetry, Fed. Aviat. Adm. Atl. City Airport, NJ 8405. (2013). doi:DOT/FAA/TC-12/53, R1.

[10] G. Linteris, M. Zammarano, B. Wilthan, L. Hanssen, Absorption and Reflection of Infrared Radiation by Polymers in Fire-like Environments, Fire Mater. 36 (2012) 537–553.

[11] J. Li, J. Gong, S.I. Stoliarov, Gasification Experiments for Pyrolysis Model Parameterization and Validation, Int. J. Heat Mass Transf. 77 (2014) 738–744.

[12] S.I. Stoliarov, R.E. Lyon, Thermo-Kinetic Model of Burning for Pyrolyzing Materials, in: Fire Saf. Sci. - Proc. 9th Int. Symp., 2008: pp. 1141–1152.

[13] S.I. Stoliarov, I.T. Leventon, R.E. Lyon, Two-Dimensional Model of Burning for Pyrolyzable Solids, Fire Mater. 38 (2014) 391–408.

[14] Y. Ding, M.B. McKinnon, S.I. Stoliarov, G. Fontaine, S. Bourbigot, Determination of Kinetics and Thermodynamics of Thermal Decomposition for Polymers Containing Reactive Flame Retardants: Application to Poly(lactic acid) Blended with Melamine and Ammonium Polyphosphate, Polym. Degrad. Stab. 129 (2016) 347–362.

[15] J. Li, S.I. Stoliarov, Measurement of Kinetics and Thermodynamics of the Thermal Degradation for Charring Polymers, Polym. Degrad. Stab. 106 (2014) 2–15.

[16] M.B. McKinnon, S.I. Stoliarov, A. Witkowski, Development of a Pyrolysis Model for Corrugated Cardboard, Combust. Flame 160 (2013) 2595–2607.

[17] Y. Ding, K. Kwon, S.I. Stoliarov, R.H. Kraemer, Development of a Semi-global Reaction Mechanism for Thermal Decomposition of a Polymer Containing Reactive Flame Retardant, Proc. Combust. Inst. 37 (2019) 4247-4255.

[18] P.J. Linstrom, W.G. Mallard, NIST Chemistry WebBook, NIST Standard Reference Database Number 69, (2018). doi:10.18434/T4D303.

[19] M. Försth, A. Roos, Absorptivity and its Dependence on Heat Source Temperature and Degree of Thermal Breakdown, Fire Mater. 35 (2011) 285–301.

[20] R. Siegel, J. Howell, Thermal Radiation Heat Transfer, Fourth, Taylor & Francis, New York, 2002.

[21] S.I. Stoliarov, S. Crowley, R.N. Walters, R.E. Lyon, Prediction of the Burning Rates of Charring Polymers, Combust. Flame 157 (2010) 2024–2034.